HHS Public Access

Author manuscript

Ann Neurol. Author manuscript; available in PMC 2017 December 01.

Published in final edited form as:

Ann Neurol. 2016 December ; 80(6): 834–845. doi:10.1002/ana.24776.

A Novel Missense Mutation of CMT2P Alters Transcription Machinery

Bo Hu, MD, PhD[1], **Sezgi Arpag, MS**[1], **Stephan Zuchner, MD, PhD**[2], and **Jun Li, MD, PhD**[1]

[1]Department of Neurology, Center for Human Genetic Research, and Vanderbilt Brain Institute, Vanderbilt University School of Medicine, Nashville, Tennessee

[2]Department of Human Genetics and Hussman Institute for Human Genomics, University of Miami Miller School of Medicine

Abstract

Objective—Charcot-Marie-Tooth type 2P (CMT2P) has been associated with frame-shift mutations in the RING domain of LRSAM1 (an E3 ligase). This study describes families with a novel missense mutation of *LRSAM1* gene and explores pathogenic mechanisms of CMT2P.

Methods—Patients with CMT2P were characterized clinically, electrophysiologically and genetically. A neuronal model with the *LRSAM1* mutation was created using CRISPR/Cas9 technology. The neuronal cell-line along with fibroblasts isolated from the patients was used to study RNA-binding proteins.

Results—This American family with dominantly inherited axonal polyneuropathy reveals a phenotype similar to those in previously reported non-US families. The affected members in our family co-segregated with a novel missense mutation Cys694Arg that alters a highly conserved cysteine in the RING domain. This mutation leads to axonal degeneration in the *in vitro* neuronal cell-line. Moreover, using protein mass spectrometry, we identified a group of RNA binding proteins (including FUS, a protein critically involved in motor neuron degeneration) that interacted with LRSAM1. The interactions were disrupted by the Cys694Arg mutation, which resulted in reduction of intranuclear RNA-binding proteins.

Interpretation—Our findings suggest that the mutant LRSAM1 may aberrantly affect the formation of transcription machinery. Given a similar mechanism has been reported in motor neuron degeneration of amyotrophic lateral sclerosis, abnormalities of RNA/RNA-binding protein complex may play a role in the neuronal degeneration of CMT2P.

Corresponding author: Jun Li, MD, PhD; Department of Neurology, Vanderbilt University School of Medicine, 1161 21th Avenue South, Nashville, TN 37232. jun.li.2@vanderbilt.edu.

Author contributions:
B.H. and J.L. contributed to study concept and design. B.H., S.A., S.Z., and J.L. contributed to data acquisition and analysis. B.H. and J.L. contributed to drafting the manuscript and figures.

Potential Conflicts of Interest:
Nothing to report.

Keywords

Charcot-Marie-Tooth disease; inherited neuropathy; CMT2P; LRSAM1; E3 ligase; ring finger domain; peripheral nerve; axonal degeneration; nerve conduction study

Introduction

Charcot-Marie-Tooth disease (CMT) affects one out of 2,500 people[1]. Patients with dominantly inherited CMT are separable into two groups: CMT1 and CMT2. CMT1 is characterized by slowed nerve conduction velocities and abnormally developed myelin (dysmyelination), whereas CMT2 shows axonal loss and reduced amplitude of nerve responses with normal or minimally decreased conduction velocities[2,3]. Most patients with CMTs share many phenotypic features, including chronic sensory loss, muscle weakness and atrophy in distal limbs.

Mutations in leucine rich repeat and sterile alpha motif 1 (*LRSAM1*, also called Tal or RIFLE) gene on human chromosome 9 have been associated with CMT2P, a dominantly inherited axonal type of CMT. LRSAM1 is an E3 ubiquitin ligase that consists of an N-terminal leucine-rich repeat domain (LRR), an ezrin-radixin-moezin domain (SAM), a coil-coil region, a sterile alpha motif domain (PTAP) and a C-terminal RING domain (Figure 1A). CMT2P was initially found in a non-US consanguineous family with an autosomal ***recessive*** mutation of p.Glu638AlafsX7[4]. Subsequently, three additional non-US families with ***dominantly*** inherited axonal CMT have been linked to different mutations in *LRSAM1* (Figure 1A)[5–7]. All these mutations alter a major portion of RING-domain amino acid sequence of LRSAM1 by either a frame-shift or insertion of additional amino acids (Figure 1A).

RING-based E3s are encoded by over 600 human genes and involve diverse cellular functions. The RING domain is usually typified by an amino acid sequence "C-X_2-C-$X_{(9–39)}$-C-$X_{(1–3)}$-H-$X_{(2–3)}$-C-X_2-C-$X_{(4–48)}$-C-X_2-C", where C is cysteine, H is histidine, and X is any amino acid[8]. Cysteines and histidines are highly conserved and critical in maintaining the structure of E3 proteins through binding two atoms of zinc (Figure 1C). RING-based E3s often function via ubiquitination of their targeted proteins (Figure 1B).

Here, we report a family with CMT2P. The affected members did co-segregate with a novel missense mutation that changed a highly conserved cysteine to arginine in the RING domain of *LRSAM1*. Moreover, we found that this mutation may impair the formation of transcription machinery.

Subjects and Methods

Patients

Five patients and three non-affected members from the proband's family (Figure 2) were evaluated (by J.L.) at Vanderbilt Medical Center. A sporadic case was from the University of Miami. This study was approved by the Institutional Review Board (IRB) in both institutions. A written consent was obtained from all participants.

In addition to medical history and neurological examination, the CMT neuropathy score (CMTES)[9] was obtained from most patients (listed in Table 1). The score is comprised of sensory and motor symptoms in limbs, physical findings in limb sensation and muscle strength. The electrophysiological portion of the score was omitted, which will be described separately below. CMTES ranges from 0 to 28, with higher scores indicating an increase of disease severity.

Nerve Conduction Studies (NCS)

NCS data were acquired using conventional methods[10]. For motor nerves, the distal stimulation distances for motor conduction studies were 7 cm in the arms and 9 cm in the legs. For the sensory nerves, the stimulation distance was 14 cm for median, ulnar and sural nerves but 10 cm for radial nerve.

DNA Sequencing

Next Generation Sequencing—The proband's DNA was initially evaluated by targeted gene-panel next-generation sequencing, a service provided by Medical Neurogenetics, Atlanta, Georgia. The test was performed on the Illumina HiSeq 2500 platform. Analysis used BWA and GATK software packages to align short reads and call variants. The sequencing covered >98% of nucleotides within exons that were interrogated at >20× depth. Average depth of coverage of all nucleotides within exons was approximately 350×. The sequencing targeted the following 42 genes (MIM#) that were known to relate to CMTs: AARS (601065); AIFM1 (300169); ARHGEF10 (608236); BAG3 (603883); BSCL2 (606158); CTDP1 (604927); DHTKD1 (614984); DNM2 (602378); EGR2 (129010); FGD4 (611104); FIG4 (609390); GAN (605379); GARS (600287); GDAP1 (606598); GJB1 (304040); GNB4 (610863); HINT1 (601314); HK1 (142600); HSPB1 (602195); HSPB8 (608014); INF2 (610982); KARS (601421); LITAF (603795); LMNA (150330); LRSAM1 (610933); MED25 (610197); MFN2 (608507); MPZ (159440); MTMR2 (603557); NDRG1 (605262); NEFL (162280); PDK3 (602526); PMP22 (601097); PRPS1 (311850); PRX (605725); RAB7A (602298); SBF2 (607697); SH3TC2 (608206); SLC12A6 (604878); TFG (602498); TRPV4 (605427); YARS (603623). In addition, whole mitochondrial DNA was sequenced.

Sanger Sequencing—The specific missense mutations in *LRSAM*1 and *MTMR2* were verified by Sanger sequencing in all participants. DNA of blood cells was extracted from all participants using a commercial kit (Promega #A1620). The test was performed at Vanderbilt Genome core (VANTAGE). Sequences were analyzed using Sequence Scanner (V1.0; Applied Biosystems).

NSC34 neuronal cell-line culture and primary human fibroblast culture

NSC34 cell-lines (murine motoneuron-neuroblastoma hybrid) (from Cellutions Biosystems Inc) were maintained in DMEM high-glucose medium (Cat# 11995, Thermo Fisher Scientific) supplemented with 10% FBS (Cat# 10082-147, Thermo Fisher Scientific). The cells were cultured on 100 μg/mL laminin (Cat# 23017-015, Thermo Fisher Scientific) coated coverslips in 24-well plates. This cell-line has been extensively characterized to document its spinal motor neuron features[11].

Skin biopsies of the proband and sex/age matched control were obtained in the Neurology Clinic of Vanderbilt University Medical Center. Tissues were washed in PBS supplemented with penicillin and streptomycin, cut into small pieces, digested overnight in DMEM high-glucose medium supplemented with 20% FBS and 0.6 mg/ml collagenase II (Cat# LS004205, Worthington Biochemical), and cultured in DMEM/20% FBS. Fibroblast outgrowth started at day 3 to 5. The remaining skin pieces were removed after one week. Culture fibroblasts were allowed to grow into 90% confluence.

CRISPR/Cas9 knockout of *LRSAM1* in NSC34 cell-line

CRISPR/Cas9 constructs were purchased from GeneCopoeia (Rockville, MD, USA). Their designs will be detailed. The NSC34 were transfected with CRISPR/Cas9-mCherry-*LRSAM1* vector by using Effectene (Cat#301425, Qiagen). After 3 days, cells were seeded as single colonies (one cell/well) in 96-well plates. After 2-3 weeks, clones were selected based on immunoblot.

Plasmids and transfection

Human *LRSAM1* plasmid (Genebank ID: BC009239; plasmid 1XHA-*LRSAM1*) was purchased from ABM (Cat# PV024451). Mutations were created using site-directed mutagenesis (primers for the reaction: F 5′-TGTGGCCACGTCCGCTGCTGCCAGC-3′; R 5′-GCTGGCAGCAGCGGACGTGGCCACA-3′). pcDNA3-EGFP was from Addgene. Primers for *LRSAM1* insertion: F: 5′-CGGGGTACCATGCCGCTCTTCTTCCG-3′, R: 5′-CATCTACCACAGCAGCacGCGGCCGCTAAACTAT-3′. KpnI site was added. The stop codon was deleted. Two extra bases were added to avoid frame shift. Following ligation and transformation to DH5a cells, the accuracy of the plasmids was verified by DNA sequencing. The plasmids were transfected into NSC34 cells by using Effectene (Cat#301425, Qiagen).

Protein Pull-down Assay with Protein Mass Spectrometry

Protein lysates were collected from NSC34 cells transfected with *LRSAM1* plasmids. 10μl of anti-GFP magnetic beads (from Vanderbilt Antibody and Protein Resource core) were added to each sample. These were rotated overnight at 4°C. Beads were washed extensively in RIPA buffer. After washing, beads were collected and resuspended in 20μl of protein sample buffer for the study of Mass Spectrometry below.

Shotgun proteomic analysis of eluate was performed by first partially resolving eluted proteins about 1.5cm using a 10% Novex precast gel, excising the protein region, and then performing in-gel tryptic digestion to recover peptides. These peptides were analyzed via MudPIT (Multidimensional Protein Identification Technology) as described[12]. Briefly, digested peptides were loaded onto a biphasic pre-column consisting of 4cm of reversed phase (RP) material followed by 4cm of strong cation exchange (RP) material. Once loaded, this column was placed in line with a 20cm RP analytical column packed into a nanospray emitter tip directly coupled to a linear ion trap mass spectrometer (LTQ). A subset of peptides was eluted from the SCX material onto the RP analytical via a pulse of volatile salt; those peptides were separated by an RP gradient and then ionized directly into the mass spectrometry. This proceeded for a total of 8 salt elution steps over the course of

approximately 16 hours of data acquisitions. Both the intact masses (MS) and fragmentation patters (MS/MS) of the peptides were collected and the peptide MS/MS spectral data searched against the mouse protein database to which the GFP fusion protein and common contaminants had been appended using Sequest[13]. Resulting identifications were then collected and filtered using Scaffold (http://www.proteomesoftware.com).

Antibodies

Mouse monoclonal anti-FUS (Cat# 60160-1-Ig) antibody was purchased from Proteintech. Rabbit polyclonal anti-G3BP1 (Cat# A302-033A), anti-BCLF1 (Cat# A300-608A) and anti-KHDR1 (Cat# A302-110A) antibodies were from Bethyl Laboratories. Mouse monoclonal anti-LRSAM1 (Cat# ab73113) was from Abcam. Mouse monoclonal anti-HDAC3 (Cat# 3949), Rabbit polyclonal anti-TDP43 (Cat# 3448) and Rabbit polyclonal anti-β-Actin (Cat# 8457) were from Cell Signaling Technology.

Co-immunoprecipitation (co-IP) and Western blot

Nuclear or cytoplasmic fractionation of human fibroblasts or NSC34 was extracted using NE-PER® Nuclear and Cytoplasmic Extraction Reagents (Cat#78833, Thermo Fisher Scientific). Cells were incubated with primary antibodies overnight at 4°C with rotation (70 rpm). Protein G agarose beads (Cat# 15920-010, Life technologies) were added for another 2 hour incubation at 4°C. Samples were eluted with Laemmli sample buffer (Cat# 161-0737, Biorad), resolved by SDS-PAGE for immunoblotting.

Whole-cell proteins were extracted using RIPA buffer (Cat# R0278, Sigma) with proteinase/phosphatase inhibiter cocktail (Cat# 5872, Cell Signaling). Samples were loaded into SDS-PAGE gels and transferred to a PVDF membrane. The membranes were blotted with 5% non-fat milk and incubated overnight at 4°C with primary antibodies and were followed by HRP-conjugated anti-rabbit or anti-mouse secondary antibodies (Cat# AP307P or AP308P, Millipore). The immune complexes were detected by the enhanced chemoilluminescence (Cat# NEL103001, Perkin Elmer).

Immunofluorescence staining

Immunostaining was performed on cells cultured on coverslips. Cells were fixed in 4% paraformaldehyde for one hour and then permeabilized with PBS containing 5% normal serum and 0.5% Triton X-100. Cells were incubated overnight with primary antibodies at 4°C. After washing, cells were stained for one hour with secondary antibodies. The stained slides were observed under a Leica fluorescence microscope (Leica DM6000B).

Statistics

We compared continuous variables between two groups using Student's *t* test. All statistical analysis was performed using GraphPad Prism software version 6.0 or SAS 9.4 and a *P* value <0.05 was used to determine significance. The Data was presented as the mean ± SD.

Results

Phenotypic and genotypic presentation is consistent with a dominantly inherited axonal polyneuropathy – CMT2

Clinical phenotypes—Patient 0001: The proband is a 51-year-old man who first developed ankle weakness in his early 30s. He tripped himself frequently and had to wear a pair of tall boots to protect his ankles. His hands and arms were less affected. His NCS revealed a sensory motor axonal polyneuropathy. Neurological examination revealed normal mental status and cranial nerve functions. Muscle strength was 4 on MRC scale in hand intrinsic muscles and ankle dorsal flexors but 5 in other muscles. Sensation was decreased to pin prick in hands and legs up to the knees and to vibration at ankles and knees. Deep tendon reflex (DTR) were absent at ankle joints but normal in other joints.

Patient 1000: This is a 71-year-old woman who became symptomatic at 43 years of age with balance issues and multiple falls. She walked with a cane. She developed numbness in feet and distal legs but asymptomatic in hands. Neurological examination detected muscle weakness in ankle dorsal flexors (4 on MRC) but 5 in other muscles. Vibration was reduced up to knee joints. DTRs were absent in all joints.

We evaluated 3 additional affected members (0100, 1001 and 1002) who presented with phenotypes similar to the two patients above. Details are listed in Table 1. Taken together, there were several notable clinical features: (1). None had significantly foot deformities (high arch feet or hammer toes). (2). Loss of vibration sense was severe in all cases, and often up to the knee level. This appeared to be disproportional to muscle weakness. (3). Excessive pelvic swings were noticed in 3 affected members. This was presumably an indication of denervation in pelvic muscles.

Electrophysiological findings—Six affected patients were evaluated by NCS (Table 2). The findings were consistent with a sensory motor axonal polyneuropathy due to the following reasons: (1). Sensory nerve action potential (SNAP) in legs was absent in all cases. SNAP amplitudes in arms were decreased in all cases. In contrast, conduction velocities were normal except for the case #0001 showing a mildly reduced conduction velocity in the median sensory nerve due to a carpal tunnel syndrome. (2). A similar pattern of abnormalities was also observed in motor nerve conduction studies. This was particularly evident in case #1000 and 0100, which had severely decreased amplitudes of compound muscle action potentials (CMAP) but showed completely normal conduction velocities in the ulnar nerves. (3). Needle EMG was performed in case #0001 and F2088 and showed denervation in distal leg muscles. The diagnostic criteria of carpal tunnel syndrome were met in two patients (case #0001 and 1000).

DNA analysis shows a missense mutation that changes a highly conserved cysteine to arginine in the RING domain of LRSAM1

The proband DNA was initially sequenced by targeted gene-panel next-generation sequencing, a commercial diagnostic service provided by Medical Neurogenetics. This technique was briefly described in Method section. This test identified two heterozygous

missense mutations, c.(2080T>C) in *LRSAM1* on chromosome 9 and c.(1288G>C) in *MTMR2* on chromosome 11. The mutations changed cysteine to arginine (Cys694Arg) in *LRSAM1*, and glutamate to glutamine (E430Q) in *MTMR2*. In addition, whole mitochondrial DNA was sequenced and revealed no mutation.

We verified these two missense mutations using Sanger sequencer (Figure 3). Cys694Arg was only found in affected family members but absent in non-affected family members (Figure 2 and Table 1). This co-segregation between Cys694Arg in *LRSAM1* and affected individuals supported its causal role of this disease. In contrast, the heterozygous Glu430Gln (E430Q) mutation in *MTMR2* was detected in 2 affected members and 1 non-affected member but absent in 3 affected members. This random distribution strongly rejected its causal role for this disease.

Cysteine at the 694 residue of LRSAM1 is highly conserved (Figure 3). The mutation was evaluated by two servers – PolyPhen-2[14] and SIFT[15]. In a study, 80% and 82% of a group of disease-causing mutations were correctly predicted to be deleterious by the two online tools[16]. Both PolyPhen-2 and SIFT predicted that Cys694Arg was deleterious. In addition, this mutation was evaluated by MutationTaster (‘disease causing’) and the LRT score (‘deleterious’).

We searched Cys694Arg mutation in the GEM.app/GENESIS database. This NIH-supported online database stored genetic variants identified from hundreds of CMT patients, and related disorders[17]. The Cys694Arg mutation of *LRSAM1* was found in a 48-year-old man with a diagnosis of idiopathic sensory motor axonal polyneuropathy (see nerve conduction study results in F2088 of Table 2). He reported no family history.

Finally, the following analysis also supports the pathogenicity of the Cys694Arg mutation. The Cys694Arg allele was present in 1 allele out of 107784 chromosomes in the ExAC database. The EVS database does not list this allele in 13000 chromosomes. The GENESIS database contains 5400 exomes. A vast majority of enrolled subjects were associated with a neurodegenerative disease, including 587 cases with CMT2. None, but F2088, had the Cys694Arg allele.

Expression of human Cys694Arg mutant LRSAM1, but not wild-type LRSAM1, in LRSAM1 null (*Lrsam−/−*) neuronal cell-line results in axonal degeneration

To further test the causal role of the Cys694Arg mutation, we have used CRISPR/Cas9 to disrupt the *Lrsam1* gene in NSC34 mouse neuronal cell-line (Figure 4). Because the transfection only took place in about 20–30% NSC34 cells, we selected multiple single cell clones. A complete knockdown of *Lrsam1* (*Lrsam1*−/− cells) was verified by Western blot in several clones, which were devoid of LRSAM1 expression (line 4 and 6 in Figure 4B). Depletion of LRSAM1 in NSC34 resulted in no phenotype in culture, which was consistent with negligible phenotype observed in *Lrsam1*−/− mice[18].

NSC34 cells from two *Lrsam1*−/− clones were transfected with plasmids expressing either wild-type human LRSAM1 or Cys694Arg LRSAM1. Transfected cells were examined under phase contrast microscopy. Axons with multiple beads, a sign of axonal

degeneration[19], were manually counted. Percentage of abnormal axons was drastically increased in Cys694Arg cells, compared with that in wild-type cells (Figure 4C, D, E). This finding supports the causal role of Cys694Arg mutation in CMT2P.

Cys694Arg mutation alters formation of nuclear transcription machinery

To understand how the Cys694Arg mutation causes the disease, we combined a pull-down assay and protein mass spectrometry to identify proteins that may interact with LRSAM1. The procedure is illustrated in Figure 5A. Plasmids expressing wild-type or Cys694Arg human LRSAM1 tagged with green fluorescence protein (LRSAM1-GFP) were transfected into the *Lrsam1*−/− NSC34 cells. LRSAM1-GFP along with its interacting proteins was pulled down by magnetic beads conjugated with a specific GFP antibody or GFP interactor.

The pulled-down proteins listed in Figure 5B, including LRSAM1 itself, revealed a cluster of RNA binding proteins among the top candidates. One top candidate, FUS, has been critically involved in the pathogenesis of motor neuron degeneration in amyotrophic lateral sclerosis (ALS)[20].

We chose five RNA-binding proteins (FUS, G3BP1, DDX1, BCLF1 and KHDR1; underlined in Figure 5B) based on their relative levels, known biological functions and availability of antibodies suitable for the co-IP experiments. Their interactions with LRSAM1 were verified in human fibroblasts or NSC34 cells by co-IP experiments. Two (FUS and G3BP1) of the five proteins were further analyzed and shown in Figure 6. FUS levels in cytoplasm were low and only pulled down a negligible amount of LRSAM1 (Figure 6A). As expected, FUS was abundant in nuclei. FUS antibodies pulled down LRSAM1 from nuclear proteins of normal fibroblasts but failed to pull down Cys694Arg LRSAM1 from fibroblasts of patients with CMT2P. A disruption of protein-protein interaction was also observed between Cys694Arg LRSAM1 and G3BP1 (Figure 6B). These changes were associated with a decrease of nuclear FUS and G3BP1 levels in CMT2P fibroblasts (Figure 6C). TDP43, another RNA-binding protein known to interact with FUS in transcription protein complex (confirmed in Figure 6A), was also decreased in the nuclei (Figure 6C, D, F). The decrease of nuclear FUS and TDP43 was further substantiated by immunostaining the human fibroblasts. The levels of nuclear FUS fluorescence intensity were significantly decreased compared with those in normal fibroblasts (Figure 6D–E). Unlike a previous study[21], we could not confirm the interaction between Tsg101 and LRSAM1 in human fibroblasts and our mass spectrometry assay even while Tsg101 was present.

Furthermore, we expressed wild-type and Cys694Arg human LRSAM1 in *Lrsam1*−/− NSC34 neuronal cell-line. Co-IP was performed. Again, we found the disruption of interaction between mutant LRSAM1 and FUS and the decrease of nuclear FUS levels (Figure 6G–H).

Taken together, the Cys694Arg mutation of LRSAM1 alters interactions between LRSAM1 and some RNA-binding proteins that are required for nuclear transcription machinery. It should be clarified that an increase of interaction between mutant LRSAM1 and other RNA binding proteins is possible. These abnormalities are expected to change the protein stoichiometry of transcription machinery, leading to the alterations of RNA metabolism[20].

Discussion

Our study has identified a family and a sporadic case who are afflicted by an inherited sensory motor axonal polyneuropathy. This disease appears to be caused by a missense mutation (Cys694Arg) in *LRSAM1.* This conclusion is supported by the following evidence: (1). The affected individuals are co-segregated with the mutation. (2). Although CMT2P has not been reported in the American population, four previously reported non-US families from Canada, England, Germany and Cyprus displayed a phenotype similar to the American family[4–7]. (3). A sporadic case with the same mutation shares a phenotype similar to our family. (4). The Cys694Arg allele changes a highly conserved cysteine that resides in the RING domain of LRSAM1. Studies have shown that these conserved cysteines are critical for the function of any E3 ubiquitin ligase in general[8]. (5). Mutant LRSAM1, but not wild-type LRSAM1, caused axonal degeneration in culture neuronal cell-line with endogenous LRSAM1 depleted by CRISPR/Cas9.

Other than family history, our patients are clinically non-distinguishable from patients with idiopathic axonal polyneuropathy (IAP). Case F2088 with a sporadic axonal polyneuropathy further highlights this point. Given the high prevalence of IAP[22], extensive laboratory work-up would result in high costs to search for an etiology. With the remarkable advance of DNA sequencing technology and the declining price for DNA testing, an early diagnosis using genetic testing may eliminate considerable costs in these patients. This advantage will become even more evident along with the discovery of new genetic causes for neuropathies.

To understand how Cys694Arg causes the axonal degeneration, we employed protein mass spectrometry and identified a cohort of proteins that may interact with LRSAM1. RNA binding proteins were disproportionally abundant among these candidates. Two proteins from the cohort (FUS and G3BP1) were further studied in detail for their interactions with LRSAM1 by co-IP. Interestingly, the interactions were disrupted by the Cys694Arg mutation. Their levels in nuclei were decreased in mutant cells, leading to a decreased availability of RNA-binding proteins for the formation of RNA/protein complex. While TDP43 does not interact with LRSAM1 directly, it does complex with FUS. Indeed, TDP43 levels were also reduced in the nuclei (Figure 6C, D, F).

This finding is pathogenically relevant. Both FUS and TDP43 as RNA binding proteins are known to regulate the stabilization of RNA. The protein complex may also directly regulate transcription by associating with gene regulatory elements[20]. These nuclear proteins are excluded from nuclei into the cytoplasm of motor neurons in ALS, leading to dysregulation of RNA metabolism. This has emerged as one of the most promising mechanisms in the pathogenesis of motor neuron degeneration of ALS. This mechanism is further highlighted by multiple recent observations. For instance, the most prevalent ALS mutation in *C9Orf* gene impairs nuclear transport of TDP43 through RanGAP1 complex. Correction of this transport defect rescues neuronal degeneration in ALS models *in vitro* and *in vivo*[23]. Our study implicates that mutations in CMT2P may also be involved in this mechanism by altering stoichiometry of RNA binding protein complex.

It is still unclear how mutations in the RING domain of LRSAM1 lead to the mis-localization of RNA-binding proteins from the nuclei to the cytoplasm. Ubiquitination is required for targeting certain proteins into the nuclear transport protein complex[24]. It remains to be determined whether the E3-ligase activity of LRSAM1 is required to ubiquitinate the RNA-biding proteins, such as FUS or G3BP1, and whether the ubiquitination is necessary for the nuclear transport of these RNA-binding proteins.

We have noticed that a study has shown interactions between Tsg101 and LRSAM1[21]. We could not confirm the interaction in our mouse and human cells. In addition, a recent publication shows that LRSAM1 was hardly identifiable in endosomes where Tsg101 resides[18]. Thus, this finding also does not support the interaction between LRSAM1 and Tsg101. SIMPLE (also called LITAF) was reported to interact with Tsg101[25]. However, mutations in *SIMPLE/LITAF* cause CMT1C, de/dysmyelinating polyneuropathy with slowed conduction velocity[26]. This phenotype is conspicuously different from that in CMT2P. Nevertheless, this discrepancy could be due to different types of cells used between the studies. It also makes no difference for our key findings on RNA-binding proteins.

CMT2P families reported previously were associated with frame-shift mutations or amino acid insertion[5]. While mutant LRSAM1 was expected to be produced in the three families with autosomal dominant inheritance, the phenotype in the three families was highly similar to that in the Canadian family with a recessive frame-shift mutation. The recessive mutation was claimed to eliminate the expression of LRSMA1[4]. Therefore, the disease in the later three families was interpreted as a result of dominant negative effect by the mutant LRSAM1. However, because the mutation in the Canadian family resides in the terminal portion of *LRSAM1* gene, antibody against the terminal portion of LRSAM1 may not detect the mutant LRSAM1 proteins. Therefore, it is still questionable whether the disease is related to any loss-of-function of LRSAM1. In line with this notion, deletion of *Lrsam2* in mice results in negligible phenotype[18]. Nevertheless, regardless whether gain or loss of functions of LRSAM1 in these families, these two mechanisms are not mutually exclusive. The mutant LRSAM1 may either decrease its interaction with RNA-binding proteins or gain new interacting partners.

Interestingly, a similar situation has also been observed in a familial Parkinson's disease with mutations in *Parkin* gene. Parkin is also an E3 ubiquitin ligase with a RING domain at its c-terminal. Missense mutations affecting conserved cysteine in the RING domain of Parkin have been found in patients with the inherited Parkinson disease[27]. Remarkably, a subgroup of patients with mutations in *LRSAM1* has developed phenotypes of Parkinson's disease[28].

In summary, we have identified a novel missense mutation that alters cysteine to arginine in the RING domain of LRSAM1. We have shown multiple lines of evidence suggesting that this mutation is causal for the CMT2P. Our study also shows that this mutation may affect the formation of RNA binding protein complex, a potential mechanism of neuronal degeneration in CMT2P.

Acknowledgments

This research is supported by grants from NINDS (R01NS066927 to J.L.; R01NS075764, 5R01NS072248, and U54NS065712 to S.Z.), the CMT Association, the Muscular Dystrophy Association, and the National Center for Advancing Translational Sciences (UL1TR000445). The authors wish to thank Ms. Audra Hamilton for her technical assistance and Drs. Brett Parker, Bryan Burnett, Jane Howard and Ms. Robin Yawn for assisting data collection.

References

1. Skre H. Genetic and clinical aspects of Charcot-Marie-Tooth's disease. Clin Genet. 1974; 6:98–118. [PubMed: 4430158]
2. Li J. Inherited neuropathies. Semin Neurol. 2012; 32:204–214. [PubMed: 23117945]
3. Li J. Molecular Regulators of Nerve Conduction – Lessons from Inherited Neuropathies and Rodent Genetic Models. Exp Neurol. 2015
4. Guernsey DL, Jiang H, Bedard K, et al. Mutation in the gene encoding ubiquitin ligase LRSAM1 in patients with Charcot-Marie-Tooth disease. PLoS Genet. 2010; 6
5. Engeholm M, Sekler J, Schondorf DC, et al. A novel mutation in LRSAM1 causes axonal Charcot-Marie-Tooth disease with dominant inheritance. BMC Neurol. 2014; 14:118. [PubMed: 24894446]
6. Weterman MA, Sorrentino V, Kasher PR, et al. A frameshift mutation in LRSAM1 is responsible for a dominant hereditary polyneuropathy. Hum Mol Genet. 2012; 21:358–370. [PubMed: 22012984]
7. Nicolaou P, Cianchetti C, Minaidou A, et al. A novel LRSAM1 mutation is associated with autosomal dominant axonal Charcot-Marie-Tooth disease. Eur J Hum Genet. 2013; 21:190–194. [PubMed: 22781092]
8. Metzger MB, Pruneda JN, Klevit RE, et al. RING-type E3 ligases: master manipulators of E2 ubiquitin-conjugating enzymes and ubiquitination. Biochim Biophys Acta. 2014; 1843:47–60. [PubMed: 23747565]
9. Murphy SM, Herrmann DN, McDermott MP, et al. Reliability of the CMT neuropathy score (second version) in Charcot-Marie-Tooth disease. J Peripher Nerv Syst. 2011; 16:191–198. [PubMed: 22003934]
10. Li J, Krajewski K, Shy ME, et al. Hereditary neuropathy with liability to pressure palsy: the electrophysiology fits the name. Neurology. 2002; 58:1769–1773. [PubMed: 12084875]
11. Cashman NR, Durham HD, Blusztajn JK, et al. Neuroblastoma x spinal cord (NSC) hybrid cell lines resemble developing motor neurons. Dev Dyn. 1992; 194:209–221. [PubMed: 1467557]
12. MacCoss MJ, McDonald WH, Saraf A, et al. Shotgun identification of protein modifications from protein complexes and lens tissue. Proc Natl Acad Sci U S A. 2002; 99:7900–7905. [PubMed: 12060738]
13. Yates JR III, Eng JK, McCormack AL, et al. Method to correlate tandem mass spectra of modified peptides to amino acid sequences in the protein database. Anal Chem. 1995; 67:1426–1436. [PubMed: 7741214]
14. Adzhubei IA, Schmidt S, Peshkin L, et al. A method and server for predicting damaging missense mutations. Nat Methods. 2010; 7:248–249. [PubMed: 20354512]
15. Kumar P, Henikoff S, Ng PC. Predicting the effects of coding non-synonymous variants on protein function using the SIFT algorithm. Nat Protoc. 2009; 4:1073–1081. [PubMed: 19561590]
16. Lopes MC, Joyce C, Ritchie GR, et al. A combined functional annotation score for non-synonymous variants. Hum Hered. 2012; 73:47–51. [PubMed: 22261837]
17. Gonzalez MA, Lebrigio RF, Van BD, et al. GEnomes Management Application (GEM.app): a new software tool for large-scale collaborative genome analysis. Hum Mutat. 2013; 34:842–846. [PubMed: 23463597]
18. Bogdanik LP, Sleigh JN, Tian C, et al. Loss of the E3 ubiquitin ligase LRSAM1 sensitizes peripheral axons to degeneration in a mouse model of Charcot-Marie-Tooth disease. Dis Model Mech. 2013; 6:780–792. [PubMed: 23519028]
19. Roediger B, Armati PJ. Oxidative stress induces axonal beading in cultured human brain tissue. Neurobiol Dis. 2003; 13:222–229. [PubMed: 12901836]

20. Ling SC, Polymenidou M, Cleveland DW. Converging mechanisms in ALS and FTD: disrupted RNA and protein homeostasis. Neuron. 2013; 79:416–438. [PubMed: 23931993]
21. Amit I, Yakir L, Katz M, et al. Tal, a Tsg101-specific E3 ubiquitin ligase, regulates receptor endocytosis and retrovirus budding. Genes Dev. 2004; 18:1737–1752. [PubMed: 15256501]
22. Rudolph T, Farbu E. Hospital-referred polyneuropathies–causes, prevalences, clinical- and neurophysiological findings. Eur J Neurol. 2007; 14:603–608. [PubMed: 17539935]
23. Zhang K, Donnelly CJ, Haeusler AR, et al. The C9orf72 repeat expansion disrupts nucleocytoplasmic transport. Nature. 2015; 525:56–61. [PubMed: 26308891]
24. Mahajan R, Delphin C, Guan T, et al. A small ubiquitin-related polypeptide involved in targeting RanGAP1 to nuclear pore complex protein RanBP2. Cell. 1997; 88:97–107. [PubMed: 9019411]
25. Shirk AJ, Anderson SK, Hashemi SH, et al. SIMPLE interacts with NEDD4 and TSG101: evidence for a role in lysosomal sorting and implications for Charcot-Marie-Tooth disease. J Neurosci Res. 2005; 82:43–50. [PubMed: 16118794]
26. Street VA, Bennett CL, Goldy JD, et al. Mutation of a putative protein degradation gene LITAF/SIMPLE in Charcot-Marie-Tooth disease 1C. Neurology. 2003; 60:22–26. [PubMed: 12525712]
27. Maruyama M, Ikeuchi T, Saito M, et al. Novel mutations, pseudo-dominant inheritance, and possible familial affects in patients with autosomal recessive juvenile parkinsonism. Ann Neurol. 2000; 48:245–250. [PubMed: 10939576]
28. Aerts MB, Weterman MA, Quadri M, et al. A LRSAM1 mutation links Charcot-Marie-Tooth type 2 to Parkinson's disease. Ann Clin Transl Neurol. 2016; 3:146–149. [PubMed: 26900582]

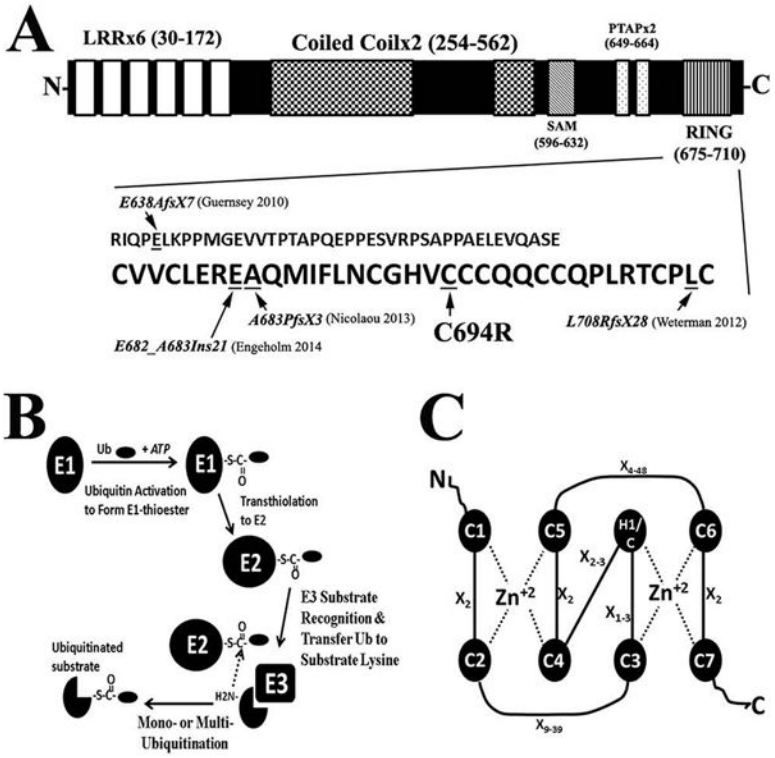

Figure 1. LRSAM1 is an E3 ubiquitin ligase

(A) A diagram in the upper panel shows different domains in LRSAM1. This is based on information provided in UniProt (http://www.uniprot.org/). Domain name followed by "x + number" indicates how many times that this domain repeats. The lower panel shows a segment of amino acid sequence adjacent to the N-terminal of RING domain (small font), followed by amino acid sequence of RING domain (large font). All four previously published mutations were marked at their starting residues. Cys694Arg (=C694R) indicates the residue that was mutated in the family of the present study. (B) This diagram shows steps of ubiquitination reaction (modified from Metzger et al BBA, 2014: 1843:47). (C) This diagram depicts a typical structural organization of E3 RING domain (Modified from Deshaies et al Annu Rev. Biochem. 2009; 78:399). Notice that highly conserved cysteins and histidine coordinate two zinc ions that are critical for the RING domain structure stabilization and interaction with E2.

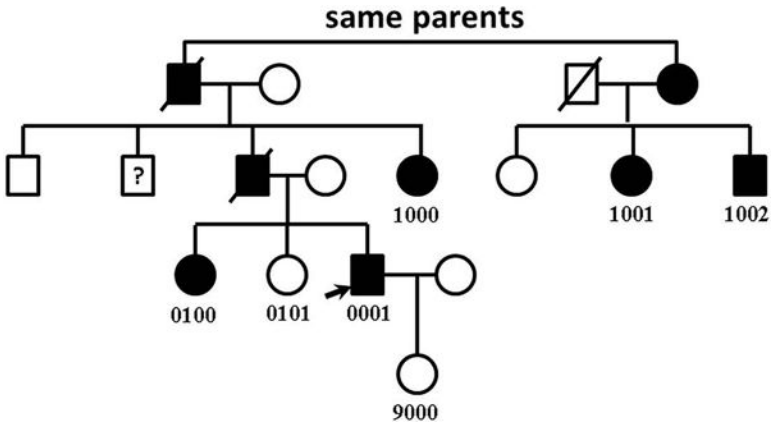

Figure 2. Pedigree of the studied family

Arrow indicates the proband. Subjects marked with numerical codes were examined clinically, electrophysiological and genetically. Members without a numerical code provided information of history and physical examination but DNA samples. Medical history and physical examination were not available for a member labelled with a question marker. Notice that there is a male-to-male transmission in the pedigree, supporting an autosomal dominant inheritance.

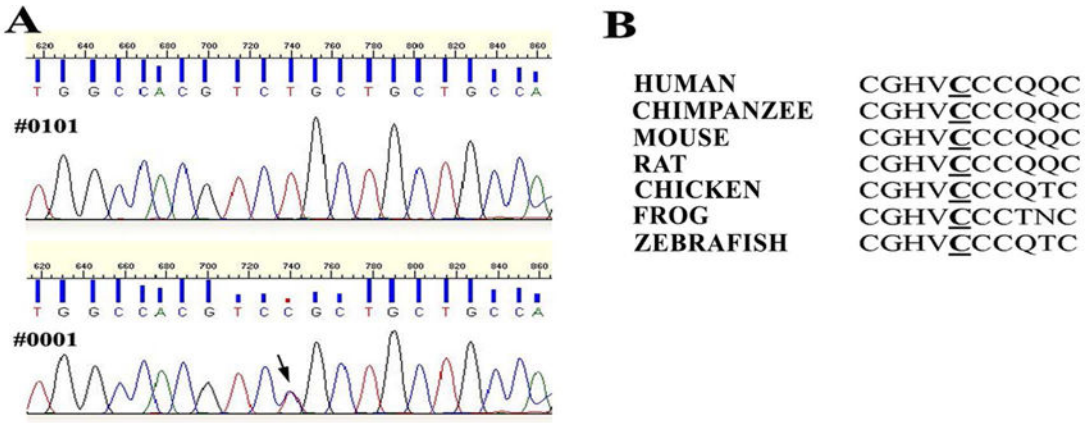

Figure 3. Sanger sequencing

(A) Original traces by Sanger sequencing were displayed for subject #0101 (unaffected) and #0001 (the proband). The mutated nucleotide was indicated by an arrow. (B) Sequence alignment shows that cysteine 694 (underlined) is conserved in all species listed.

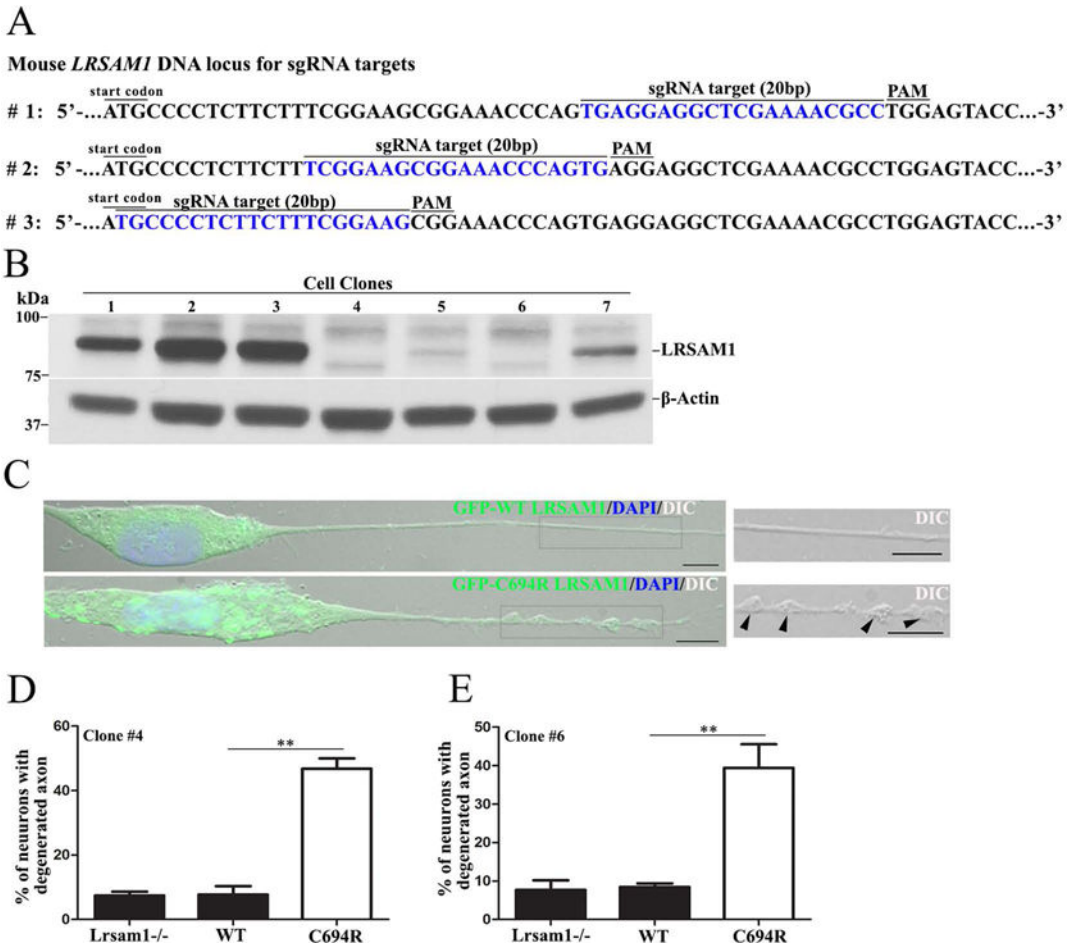

Figure 4. Cys694Arg LRSAM1 in *Lrsam1*−/− neuronal cell-line causes axonal degeneration

(A) This diagram illustrates the mouse *Lrsam1* loci. Two 20nt-targeting sequences of single-guide RNA (sgRNA) are marked in blue. Protospacer-adjacent motifs (PAM) are lined on the top. (B) Western blot of LRSAM1 in NSC34 clonal cell lines after *Cas9*/sg-*Lrsam1* transfection showed loss of LRSAM1 expression in clone 4 and 6 that were knocked down by two different sgRNA sequences. β-actin was used as a loading control. (C) *Lrsam1*−/− NSC34 cells were transfected with constructs expressing GFP-wt human LRSAM1 or GFP-Cys694Arg human LRSAM1. Three days after transfection, cells were fixed in 4% paraformaldehyde and imaged to observe neurites with beads (arrowheads). Scale bars = 10μm. (D) The percentage of cells with beads were manually counted. Degenerative cells were defined as cells that had neurites with ≥ two beads. There was a significant increase of neurites with beads in Cys694Arg *LRSAM1* cells (46.8±5.6%, n=119 cells from three wells of *Lrsam1*$^{-/-}$ cell clone #4), compared with that in *wild-type* cells (7.8±4.4%, n=133 cells from three wells) and non-transfected *Lrsam1*−/− cells (7.5±2.0%, n=168 cells from three wells). (E) The same quantification was performed in cells of *Lrsam1*$^{-/-}$ cell clone #6. Again, there was a significant difference between *wt* LRSAM1 (8.5±1.6%) or non-transfected *Lrsam1*−/− cells (7.7±4.3%) and Cys694Arg LRSAM1 (39.5±10.6%) cells (116 cells from 3 wells for *wt LRSAM1*, 124 cells from 3 wells for non-transfected *Lrsam1*−/− and 115 cells from 3 wells for Cys694Arg *LRSAM1*). $^{**}P < 0.01$.

A

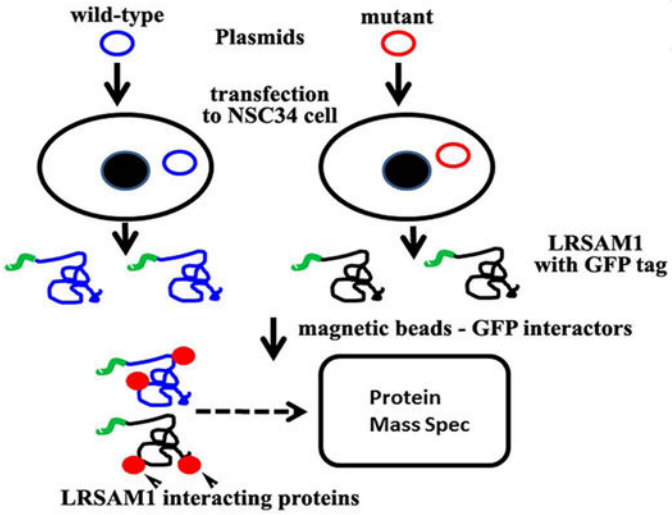

B

Top 50 candidates

Number	Protein Names	Accession Number	Number	Protein Names	Accession Number
1	SFPQ	Q8VIJ6	26	DDX3X	Q62167
2	NONO	Q99K48	27	HNRPK	P61979
3	HNRPU	Q8VEK3	28	PRC2A	Q7TSC1
4	MYH9	Q8VDD5	29	FA98A	Q3TJZ6
5	SNRPA	Q62189	30	PSPC1	Q8R326
6	DDX1	Q91VR5	31	UBP2L	Q80X50
7	PABP1	P29341	32	FBRL	P35550
8	FUS	P56959	33	DDX5	Q61656
9	KHDR1	Q60749	34	NUFP2	Q5F2E7
10	RTCB	Q99LF4	35	DHX9	E9QNN1
11	CAPR1	Q60865	36	HNRH1	O35737
12	BCLF1	Q8K019	37	TBB5	P99024
13	THOC4	O08583	38	ZFR	O88532
14	TR150	Q569Z6	39	RMXL1	Q91VM5
15	G3BP2	P97379	40	RBM33	Q9CXK9
16	FXR1	Q61584	41	ATX2	O70305
17	LS14A	Q8K2F8	42	LRSM1	Q80ZI6
18	MYH10	Q3UH59	43	HNRPQ	Q7TMK9
19	FOP	Q9CY57	44	SAFB1	D3YXK2
20	PAIRB	Q9CY58	45	RL23A	P62751
21	G3BP1	P97855	46	SLTM	Q8CH25
22	ATX2L	Q7TQH0	47	LARP1	Q6ZQ58
23	SMD2	P62317	48	HS90B	P11499
24	HSP7C	P63017	49	PRDX1	P35700
25	FMR1	E9QAT0	50	ACTC	P68033

Figure 5. Pull-down assay and protein identification with mass spectrometry

(A) Diagram to illustrate the procedure of the pull-down assay: *Lrsam1*−/− NSC34 cells were transfected with plasmids expressing wild-type human LRSAM1 (left) or mutant human LRSAM1 (right). The LRSAM1 was tagged by GFP. The protein lysates were eluted through a column containing magnetic beads conjugated with GFP antibodies. This extracted LRSAM1 and its interacting proteins. The LRSAM1 interacting proteins were then identified by the protein mass spectrometry. (B) A list of top 50 candidate proteins is displayed. Because the mass spectrometry was only semi-quantitative, it cannot provide sufficient accuracy to ascertain the difference of levels of candidate proteins between wild-type cells and mutant cells. We thus identify the top 50 proteins only based on their relative abundance, regardless whether the candidate proteins were from the wild-type cells or mutant cells. Five proteins underlined were selected for further verification by co-IP. This selection was based on their relative abundance, known biological functions and availability of antibodies suitable for co-IP experiments.

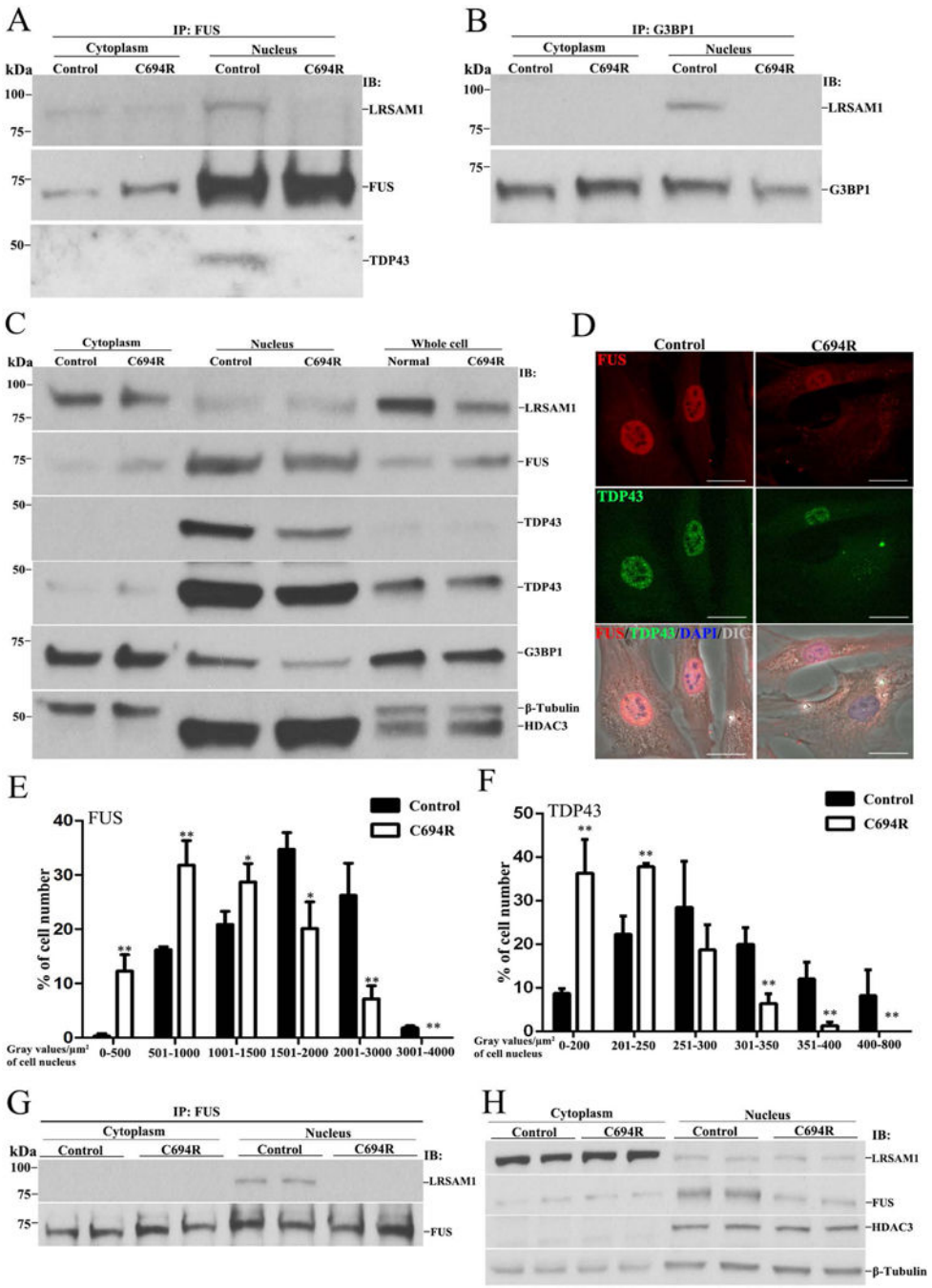

Figure 6. Cys694Arg mutation disrupts interactions between LRSAM1 and RNA-binding proteins

(**A**) Cytoplasmic and nuclear fractions were extracted from normal and Cys694Arg human fibroblasts. Proteins were immunoprecipitated (IP) with anti-FUS antibody and the precipitated proteins were immunobloted (IB) with anti- LRSAM1 and anti-FUS antibody. FUS antibody was able to pull down LRSAM1 in nuclear fractions of normal fibroblasts but failed to pull down LRSAM1 in the nuclear fractions of Cys694Arg fibroblasts. (B) IP using anti-G3BP1 antibody was carried out in cytoplasmic and nuclear fractions from the

fibroblasts. The G3BP1 antibody was able to pull down LRSAM1 in cytoplasm and nuclear fractions of control fibroblast cells but failed to do so in Cys694Arg fibroblasts. (C). Although TDP43 does not directly interact with LRSAM1, it is well known to form protein complex with FUS. We thus tested if the TDP43 is also decreased in the nuclei. Whole cell, cytoplasmic and nuclear proteins were extracted from the fibroblasts and examined by Western blot for levels of LRSAM1, FUS and G3BP1. β-Tubulin was included as a loading control of the whole cell and cytoplasmic extracts. HDAC3 served as a loading control of the nuclear extracts. Note that the row 4 was an over-exposure. In order to clearly show the difference between normal and mutant cells, we also displayed the image with a low exposure in the row 3. (D) The fibroblasts were stained with antibodies against FUS. There was a decrease of FUS immunoreactivity in the nuclei of Cys694Arg fibroblasts, compared with those in normal fibroblasts. Nuclei were also stained by DAPI. Scale bars = 10μm. (E–F) Fluorescence intensity of FUS and TDP43 were quantified from nuclei of fibroblasts. The FUS and TDP43 intensity in Cys694Arg fibroblast cells had a left shift toward higher levels (n=390 from three wells), compared to those in normal fibroblasts (n= 417 from three wells). $*P < 0.05$, $** P < 0.01$. (G) *Lrsam1*−/− NSC34 cells of clone #4 was transfected with constructs expressed wt-human LRSAM1 or Cys694Arg LRSAM1. Three days after transfection, cell colonies were selected to ensure the uniformity of LRSAM1 expression in all cells. Protein lysates from cytoplasmic or nuclear fractions were used for IP. FUS antibody was able to pull down LRSAM1 in the nuclear fractions of wt-LRSAM1 cells but failed to pull down LRSAM1 in the nuclear fractions of Cys694Arg cells. (H) Western blot of LRSAM1 and FUS was performed in the cytoplasmic or nuclear fractions extracted from wt-LRSAM1 or Cys694Arg cells. The levels of nuclear FUS were decreased in the Cys694Arg cells compared with that in wt-LRSAM1 cells.

Table 1

Clinical features in patients with CMT2P.

Code	0001	1000	0100	1001	1002
Sex/Age	M/51	F/71	F/56	F/66	M/61
Onset age	30s	43	20s	40s	30s
Weakness	HI[1] 4; ADF[2] 4	ADF 4	ADF 4	none	ADF 4
Vibration[3]	knee	knee	knee	knee	knee
Pin Prick	knee	mid calf	mid calf	distal leg	ankle
DTR[4]	ankle	all joints	all joints	all joints	all joints
F. Deformities[5]	none	none	none	none	none
PSw[6]	no	yes	yes	yes	no
CMTES[7]	18	7	12	8	6
LRSAM1[8]	C694R	C694R	C694R	C694R	C694R
MTMR2[9]	E430Q	no	E430Q	no	no

[1] HI = hand intrinsic muscles;

[2] ADF = ankle dorsal flexor;

[3] Level of abnormal vibration;

[4] DTR = joints with absent deep tendon reflex;

[5] F. Deformities = foot deformities (high arch feet or hammer toes);

[6] PSw = pelvic swing;

[7] CMTES = an examination sub-score from CMTNS, which omitted NCS;

[8] C694R = Cys694Arg. Note that the C694R mutation is absent in all tested non-affected members (0101 and 9000).

[9] MTMR2 = mutation in myotubularin related protein-2 gene. Glu430Gln = E430Q.

Table 2

Electrophysiological findings

Code	Sensory Nerve Conduction			Motor Nerve Conduction		
	Median	**Ulnar**	**Sural**	**Median**	**Ulnar**	**Peroneal**
	DL(ms)/Amp(μv)/CV(m/s) [1]			***DL(ms)/Amp(mv)/CV(m/s)***		
Norm [2]	3.5/22.0/50	3.5/10.0/50	4.4/6.0/40	4.4/4.0/49	3.3/6.0/49	6.5/2.0/44
0001	3.6/10.0/46	2.5/7.0/55	nr [3]	4.3/10.2/52	2.7/8.2/61	5.6/1.5/33
1000	nr	nr	nr	6.3/2.7/61	4.4/3.7/82	6.3/1.3/32
0100	nr	nr	nr	3.9/8.8/58	3.2/2.5/72	nr
1001	ND [4]					
1002	nr	nr	nr	4.6/7.6/52	3.4/13.2/54	7.6/2.4/35
F2088 [5]	3.2/5.0/50	ND	nr	3.4/8.6/57	ND	6.1/0.3/42

[1] DL(ms)/Amp(μv)/CV(m/s) = distal latency (ms)/amplitude (mv)/conduction velocity (m/s). All numbers in each column were listed in this sequence. Letters in the parenthesis represent the units of the measurement;

[2] Norm = normative values. For DL, the listed numbers are the upper limit of normal. For Amp and CV, the listed numbers are the lower limit of normal.

[3] nr = no response;

[4] ND = not done;

[5] F2088: This was the code for the patient from University of Miami